Available online at www.sciencedirect.com

ScienceDirect

Procedia Manufacturing 34 (2019) 754–763

Procedia MANUFACTURING

www.elsevier.com/locate/procedia

47th SME North American Manufacturing Research Conference, Penn State Behrend Erie, Pennsylvania, 2019

Deposition path planning for material extrusion using specified orientation fields

Joseph R. Kubalak, Alfred L. Wicks, Christopher B. Williams*

Department of Mechanical Engineering, Virginia Tech, Blacksburg, VA 24060, USA

Abstract

The thermal characteristics of the material extrusion additive manufacturing (AM) process produce weak bonds between layers and adjacent depositions, resulting in an overall anisotropic mechanical performance. Design for AM guidelines advise printing load-bearing parts such that load is applied strictly along the deposition paths, but this can be difficult to achieve with complex loading conditions. Recent works have explored toolpath generation techniques capable of generating deposition paths that are aligned with complicated load paths, but the methods rely on assumptions about the shape of the load paths relative to the geometry. In this paper, the authors present an algorithm for generating deposition paths for any arbitrary geometry and anticipated load paths. Deposition paths are planned using a streamline placement algorithm - commonly used for visualizing fluid flow fields - that treats the load paths as a velocity field. The algorithm is demonstrated on an example geometry, and the volumetric coverage of the resulting toolpath is compared to a toolpath generated using a standard toolpath planning technique. Through this comparative study, it is demonstrated that the toolpath resulting from the authors' proposed algorithm is able to follow the load paths while still achieving similar volumetric coverage to the standard toolpath.

Keywords: tailored deposition alignment; orientation field; streamlines; additive manufacturing; material extrusion

1. Introduction

Material extrusion (ME) additive manufacturing (AM) systems typically utilize 3 degree of freedom (DoF) platforms to enable linear motions in the X, Y, and Z directions [1]. This limited range of motion constrains the fabrication process to the stacking of XY-planar layers along the Z-axis. While enabling significant freedom in the design of part geometry, the thermal characteristics of the ME process result in poor bonding between the individual layers, weakening the part along the build direction [2]. To a lesser extent, the bonds between adjacent depositions are subject to the same phenomenon. As a result, the final part will demonstrate anisotropic mechanical properties that are dependent on the global build direction and the infill pattern used in each layer [3].

Typically, 3-DoF toolpath planners (often referred to as slicers) operate by dividing the desired geometry into 2D contours along the build direction [4]. The contours are then filled with deposition paths through a variety of methods, depending on the specific slicer and configuration settings. This produces a series of 2D layers, filled with deposition paths, ordered in terms of ascending Z-height [5]. When printing load bearing parts, the deposition paths within each layer are ideally oriented by the designer such that loads are applied along the deposition directions and not across the inter-layer or inter-deposition bonds [6]. For example, to print the L-bracket geometry shown in Figure 1a for optimal mechanical performance, the deposition paths should align with the load paths produced by the tensile loads (Figure 1b). The directions of these load paths form an orientation field, as shown in Figure 1c. While this example orientation field is relatively simple, orientation fields for end-use applications are often non-planar and consist of a large number of different directions.

Due to rigid infill patterns and limited tunable parameters (e.g., raster angle), typical slicing tools have difficulty following

* Corresponding author. Tel.: +1-540-231-3422
E-mail address: cbwill@vt.edu (Christopher B. Williams).

10.1016/j.promfg.2019.06.209

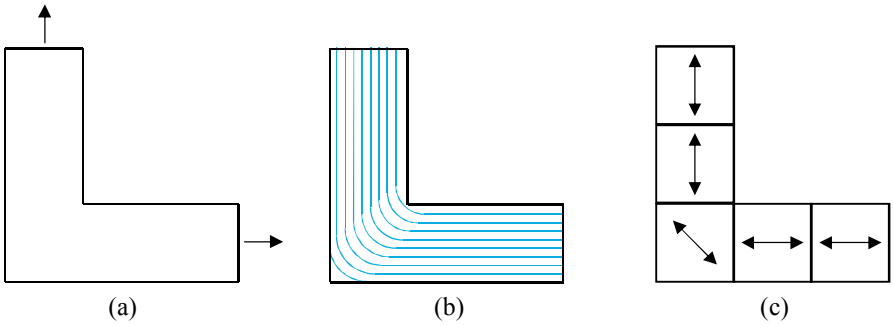

Fig. 1: (a) L-bracket geometry with a tensile load applied to each arm of the bracket, (b) load paths created by the tensile loads, and (c) a discretized orientation field that represents the load paths.

complex orientation fields. To address this gap, researchers have developed algorithms that attempt to align toolpaths with orientation fields. For instance, Hoglund and Smith generate toolpaths from topology optimization (TO) results, where a geometry is simultaneously optimized with an orientation field that denotes the optimal deposition directions for strength [7]. In their work, the orientation field follows the density features of the geometry according to Michell's truss theorem [8]. Using this feature, they chose appropriate slicer settings to produce toolpaths consisting of exclusively contour paths that coincidentally follow the orientation field. Liu and Yu developed a level-set TO method where deposition paths were created by changing the threshold for the level-set, producing concentric deposition paths within an external contour [9]. In both works, the orientation field was not explicitly used for toolpath planning; it was used implicitly by assuming the orientation field followed the density features of the design space. Such implicit methods are not generalizable to any geometry and orientation field, as the orientation field does not necessarily need to follow the density features (e.g., [10]). A more robust method for deposition path planning would be to directly use the orientation field to propagate deposition paths.

1.1. Multi-Axis Toolpath Planning

The concept of aligning deposition paths with orientation fields becomes even more valuable when using multi-axis deposition systems that allow the deposition head and printed part to reorient relative to each other. Unlike 3-DoF platforms, which are only able to follow XY-planar load paths, the freedom of motion afforded by multi-axis systems enables the alignment of depositions with 3D load paths. This capability provides significant opportunities to optimize a part's toolpath and thus its mechanical properties, but toolpath planning techniques that leverage this freedom are limited. Specifically, multi-axis toolpaths must be planned for the entire volume rather than single layers, and the ability to reorient introduces collision concerns between the tool head and previously deposited material. To circumvent these issues, existing performance-focused multi-axis deposition techniques are limited to fabricating surface geometries that are known beforehand to not have issues with collisions. For instance, Yerazunis et al. fabricated hemispherical pressure caps on a 5-DoF system where deposition paths were aligned with stress paths [11]. These aligned specimens ruptured at pressures 4.5 times greater than specimens fabricated using typical 3-DoF printing. Tam and Mueller printed optimized 2.5D surface geometries using a 6-DoF robotic arm, demonstrating a 76% improvement in ultimate compressive load over similar geometries fabricated using strictly XY-planar layers [12]. Previous work from the authors investigated the effects of conformal surface printing, similar to a composite layup process, facilitated by a 6-DoF robotic arm [13]. Tensile specimens fabricated with the surface reinforcement outperformed specimens without reinforcement by 59% in yield tensile stress.

The ability for multi-axis ME to deposit material out of the XY-plane provides an opportunity to truly optimize a part's performance as it allows for the alignment of deposition paths with orientation fields in all three dimensions. In the cases of [11, 12], the orientation fields were explicitly created. Analysis tools determined lines of principal stresses and deposition paths were propagated along those lines. For [13], the orientation field was not explicitly created, as the load paths were simplified in the tensile specimen geometry, but the expected load paths still informed the toolpath.

While these works demonstrate the potential to improve mechanical performance with multi-axis deposition, a generalized toolpath planner that is informed by performance-driven orientation fields does not exist. Existing methods that have been used for 3-DoF printing (e.g., the contour [7] and level-set [9] methods) are not applicable to 3D orientation fields. The features extracted using these methods would be 3D surfaces, rather than printable 2D contours. Instead, a volumetric approach to toolpath planning would be more suitable for application to both planar and multi-axis geometries and orientation fields. Ezair et al. outlined a volumetric method for generating deposition paths using a series of extracted isosurfaces [14]. Although their method allowed predetermined curvatures to define the shape of the generated deposition paths, only simple

curvatures that kept each deposition path along a unique trajectory were demonstrated. For more complex orientation fields, such as those demonstrated in [7], prescribing the deposition path shapes is not feasible.

1.2. Toolpath Planning for Orientation Fields via Streamlines

Orientation fields (e.g., Figure 1c) feature discrete, discontinuous vectors. Although these element-based orientation fields have been printed using a material jetting process [10], they are unsuitable for printing directly via ME. Deposition paths could be propagated through each element individually, but this would introduce weak interfaces between neighboring elements [15]. Therefore, some method of connecting these discrete elements with continuous deposition paths is necessary to achieve the desired mechanical performance. To address this issue, the authors present the volumetric deposition path generation (VDPG) algorithm as a toolpath generation scheme capable of following any orientation field (Section 3). VDPG builds on streamline placement algorithms, which are typically used to visualize complex fluid flows in the field of computational fluid dynamics (CFD). Streamline placement algorithms (reviewed in Section 2) operate by advecting discrete particles through the design space and tracking their motion to create streamlines that accurately follow the input flow field. These algorithms have the same criteria for success as ME toolpaths (i.e., long, continuous streamlines with even spacing), and the resulting streamlines are easily converted to deposition paths for the ME process. In this work, an analog to CFD flow fields is produced using the prescribed deposition directions from a TO algorithm. By directly using the orientation field to create deposition paths, VDPG has no restrictions on the shape of the orientation field with respect to the geometry and predetermined path shapes are not required.

To validate the VDPG algorithm, the authors present its application to a 2.5D Messerschimitt-Bölkow-Blohm (MBB) beam, a standard TO problem, in Section 4. In this case study example, the geometry is first optimized using a TO algorithm, previously developed by the authors, with considerations for 3D material orientations [16]. The algorithm produces an element-based geometry with orientations defined within each element, creating an orientation field. Although the TO algorithm enables 3D material orientations, the scope of this paper is limited to validating the VDPG algorithm using arbitrary geometries with planar orientation fields. In Section 5, the authors present an outline and path for extending the VDPG algorithm to multi-axis loading conditions and toolpaths.

2. Streamline Placement Algorithms

In the field of fluid flow analysis, CFD tools have been created to solve for the flow fields of arbitrary geometries and their associated boundary conditions. Using a CFD software, flow velocities are obtained throughout the geometry, either within the discretized elements of the design space or at their nodes [17]. Parsing these flow velocities can be difficult for a user, especially for turbulent or otherwise complex flows [18]. This difficulty spawned an area of research focused on conveying the motion of fluid flows in an easily understandable fashion by utilizing streamlines to depict the motion in a visual manner.

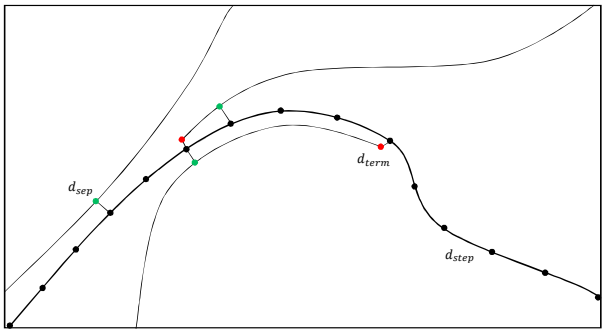

Fig. 2: An initial streamline (thick) is advected and seed points (green) are created. If new streamlines (thin) get too close to existing streamlines, they are terminated (red).

As reviewed by McLoughlin et al., a popular method for obtaining these streamlines is to place discrete particles in the flow field and track their motion [19]. There are a number of different algorithms dedicated to the creation of streamlines, but many of them follow the same general process (shown in Figure 2). First, an initial particle is tracked through the flow field. Additional seed points are propagated from the created streamline that are then also tracked to create streamlines. These streamlines are used to propagate more seed points, and the process repeats. This general structure has been used for a variety of fluid flow problems including steady [20, 21] and unsteady [22] flows and is also applicable to 3D flow fields [23, 24]. Similar placement algorithms have also been applied to remeshing algorithms based on feature curvature [25] and line rendering for image shading [26].

Particle tracking is performed through the numerical integration of the advection equation (Equation 1), where x is a point in the flow field with a flow velocity $V(x)$. The choice of integrator varies between works, with common choices being the Runge-Kutta (RK) and Euler methods [27, 28]. These integration schemes provide smooth, high quality streamlines and enable relatively large step sizes (d_{step}) to minimize computation cost.

$$\frac{\partial x}{\partial t} = V(x) \tag{1}$$

Creating new seed points in the design space often takes place at each integration step [29]. For each new position along a given streamline, a set of seed points is created some desired distance (d_{sep}) away from the streamline. This strategy ensures that, at least for the first time step, each streamline has the desired separation. Recent works have pointed out that this

method of seeding can result in collections of short streamlines, as the initial proximity to other streamlines can cause rapid termination. For these reasons, other seeding strategies have been developed such as farthest point [28] and double-queueing [20].

During advection, the streamline is monitored in regards to its proximity to other streamlines [30]. If the current streamline enters within some distance (d_{term}) of another streamline, its advection is stopped to prevent overlapping streamlines that would confuse the visualization of the flow field. In order to improve the appearance and coverage of the streamlines, the termination distance is typically shorter than the separation distance used for seeding [31]. This process of advection and seeding results in volumetric coverage of the flow field in streamlines approximately separated by d_{sep}.

3. Volumetric Deposition Path Generation Algorithm

The VDPG algorithm is driven by the need for a printed part to meet some performance criteria or metric. Analysis and design tools (e.g., finite element analysis, TO, etc.) can be used to define an orientation field to meet that criteria, and the VDPG algorithm then propagates deposition paths through that field. In this work, both the part geometry and its orientation field are obtained through the TO algorithm described in [16]. Although VDPG was designed with TO in mind, the input to the algorithm (a geometry and orientation field) could be generated by other means.

VDPG generates deposition paths volumetrically through the geometry using a streamline placement algorithm, where the specified orientations are used as streamline advection velocities ($V(x)$ in Equation 1) with a unit magnitude. A high-level overview of the VDPG algorithm is shown in Figure 3 with highlighted processes detailed below.

1. **Map orientations to nodes.** To produce smooth streamlines, the orientations are mapped to the nodes of the discretized geometry by averaging the orientations of each node's neighboring elements. Initial testing of the algorithm directly used the element orientations as the particle velocities, but it lead to unsatisfactory results. The instantaneous velocity transitions across the element interfaces produced streamlines that often converged at those interfaces and terminated (shown in Figure 4a).

   The orientation field is bi-directional, as shown in Figure 1c, and averaging the orientations without consideration could produce undesirable results. A deposition can start and end from either of its two end points and effectively result in the same deposition. This bi-directional nature implies that a particle in the field could travel along two parallel, but opposing, velocity vectors. Only one of these vectors is represented by the element's orientation though, creating the possibility of two opposing velocity vectors being averaged together to produce a zero result. To prevent this, the element orientations relevant to each node are repaired as shown in Figure 5. One element's orientation is fixed and the other orientations are compared to it. Orientations that oppose the fixed orientation (i.e., form negative dot products) are negated, and these repaired orientations are averaged and mapped to the selected node. As this strategy can produce different results based on the chosen fixed element, the most dense element (according to the TO algorithm) surrounding the node is selected as the fixed element to minimize the impact on the orientation field.

   During advection, the particle velocity is determined using the eight-node hexahedral shape function [32]. This method of mapping nodal velocities to a particle velocity produces a more continuous velocity field, mitigating the harsh transition zones between elements. Streamlines developed using this method, shown in Figure 4b, qualitatively demonstrate smoother paths through the velocity field.

2. **Generate initial seed points.** A heuristic initial seeding strategy is used in this work that places a seed point in the center of each element in the design space. This scheme was employed to ensure streamlines were generated within each element. These seed points are used to initialize the open list of seed points.

3. **Create seed points.** During advection, seed points are placed at each integration step, separated by a distance d_{sep} from each other and the integration step. By setting d_{sep} to the expected deposition width, the seed point spacing is similar to a 100% infill in a typical slicer (i.e., the cross-sections of adjacent printed depositions touch at a singular point). In order to place the largest number of seeds possible, a pattern of six seed points is created at each step, forming a hexagon around the integration point (Figure 6) [23].

4. **Advect streamline.** In this work, a fourth-order RK integrator was used to numerically integrate the advection equation. This integrator was chosen for its prevalence in streamline literature [20, 24] and for its ability to efficiently generate smooth streamlines, but another integration scheme could be used. The RK integrator uses a series of intermediate points during each step to produce a more accurate result. At each of these intermediate points, the nodal velocities are mapped to the particle using the shape function method as previously described.

   Due to the bi-directional nature of the orientation field, each point in the orientation field has two possible velocities with the same magnitude but opposite directions. Each velocity would create a different, but equally valid, streamline. This is not a necessary consideration for typical fluid flow problems as a given point in the flow can only have a single velocity. To promote smooth streamlines, dot products are formed between the streamline trajectory in the previous time step and the two opposing velocity vectors at the current time step (Figure 7). Only one of the dot products will be positive, and that velocity vector is chosen for the current step.

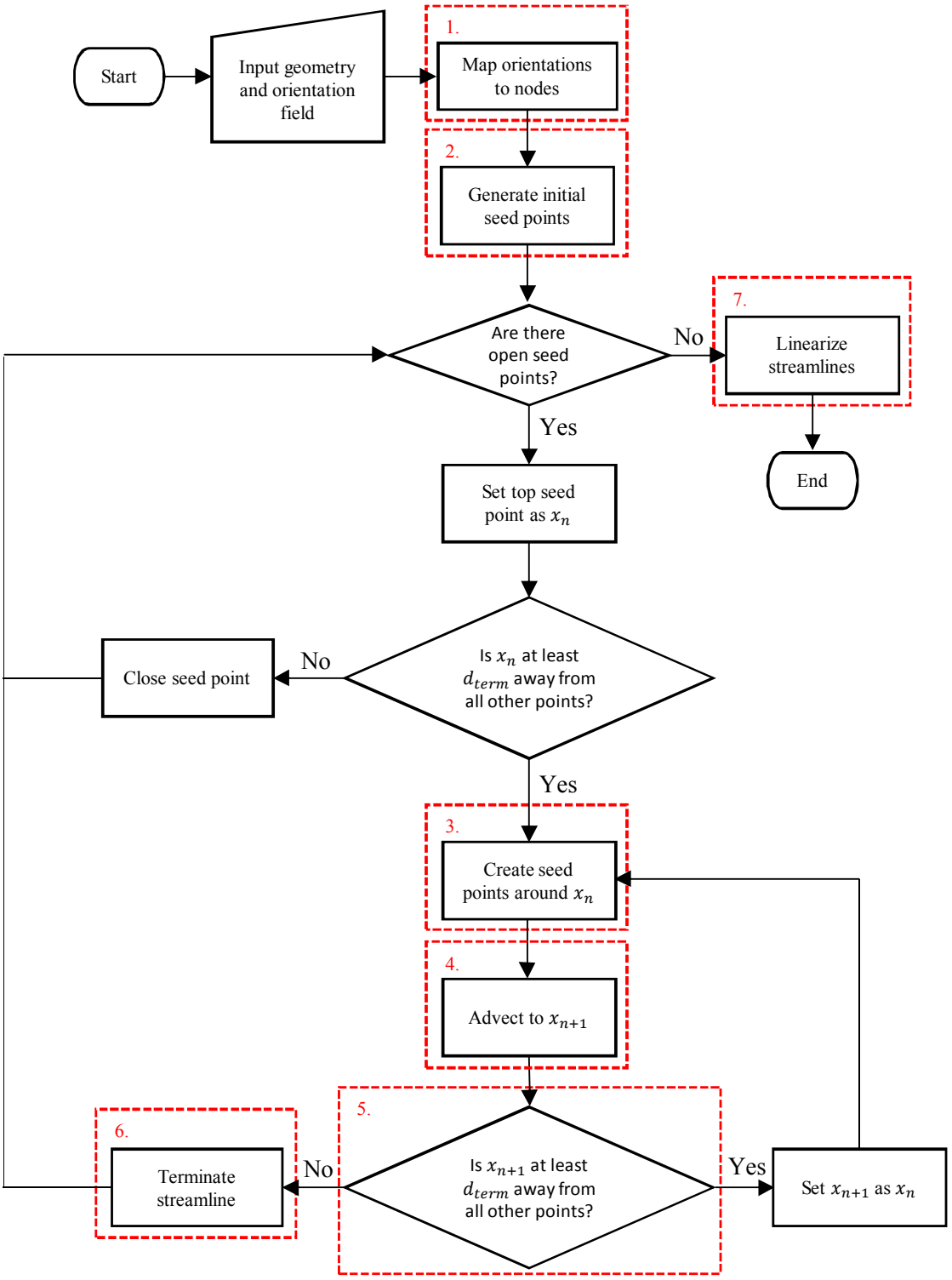

Fig. 3: VDPG algorithm flowchart. Highlighted processes are elaborated in the text.

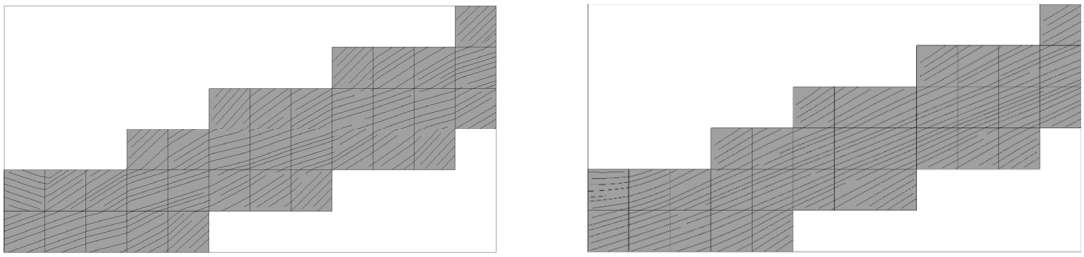

(a) (b)

Fig. 4: Velocities are determined during integration via (a) the element's orientation and (b) mapped nodal orientations. The streamlines are smoother using nodal orientations and are less prone to termination near the element interfaces.

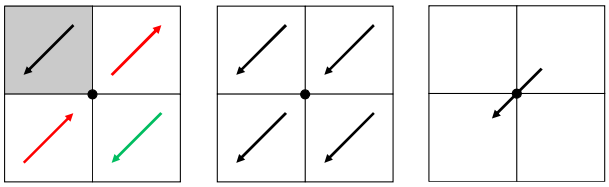

(a) (b) (c)

Fig. 5: Process for mapping velocities to the nodes. (a) A fixed element (gray) is selected and orientations that form negative dot products (red) are found, (b) orientations with negative dot products are negated, and (c) the repaired orientations are then mapped to the node.

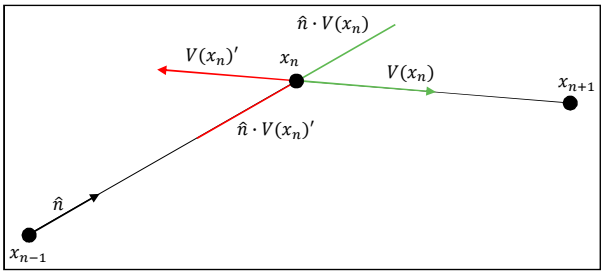

Fig. 7: To promote smooth deposition paths, the velocity is selected such that the dot product of the new velocity, $V(x_n)$, and the direction of the previous step, $\hat{n}$, is positive.

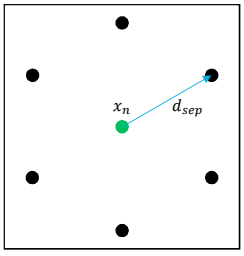

Fig. 6: New seed points are created using a hexagonal pattern around the new integration point (x_n). The plane that contains the seed points shares its normal with the current velocity of the streamline.

5. **Validate new point.** In the context of ME, overlapping streamlines would result in the over-extrusion of material or possibly the collision of the tool head with previously printed material. To prevent this situation, as the streamline is advected, each integration point must be checked to ensure it is not within the termination distance (d_{term}) of a point on another streamline. If the integration point of the current step is found to be within the termination distance of an existing point, it is not saved to the current streamline.

6. **Terminate streamline.** If the streamline comes within d_{term} of another streamline, advection is stopped to prevent overlapping deposition paths. The streamline is saved, all of the developed seed points are added to the open list, and the initial seed point used is removed from the open list. For printers with minimum feature sizes (L_{min}), the streamline can be checked for length to ensure it is above that minimum limit. If the streamline is found to be below L_{min}, the initial seed point is still removed from the open list but the streamline is not saved nor are the generated seed points added to the open list.

7. **Linearize streamlines.** The streamlines resulting from the placement algorithm are smooth, spline-based curves. Depending on the capabilities of the fabrication process, it is likely that only linear tool head movements are possible, making these streamlines difficult to fabricate. To accommodate, the streamlines are linearized using the chord length method (CLM) [33]. CLM spans the streamline with a series of line segments that attempt to minimize chord height (i.e., the maximum distance between the line segment and the spanned portion of the streamline). The maximum allowable chord height is set us-

ing the d_{lin} parameter. The value of d_{lin} is important as, with large values, it is possible to produce overlapping linearized streamlines when the spline-based streamlines did not overlap.

VDPG can be tuned to a specific deposition process through a number of parameters. d_{sep} corresponds to the expected deposition width and height, and d_{term} should be tuned to the lowest value that does not result in unacceptable over-deposition to promote full coverage of the expected streamline volume. d_{step} is tuned along with the chosen integration scheme to create streamlines with the desired levels of fidelity and speed. Both d_{lin} and L_{min} depend on the capabilities of the process, specifically the minimum printable feature size.

The result of the VDPG algorithm is a set of linearized deposition paths that follow the desired orientation field and volumetrically fill the input geometry. For planar printing, these deposition paths can then be ordered in terms of ascending Z-height to produce a printable toolpath.

4. Algorithm Validation

A 2.5D MBB beam geometry was selected to validate the VDPG algorithm for its prevalence in AM optimization literature [34, 35, 7]. The geometry and orientation field were developed using a TO algorithm with considerations for 3D material orientations [16]. The TO algorithm is described briefly in Section 4.1 and the VDPG algorithm is validated using the MBB beam geometry in Section 4.2. Two metrics are used to evaluate the resulting toolpath: i) the inter-deposition spacing and ii) the volumetric coverage of the deposition paths. The inter-deposition spacing is used as a measure of proper streamline termination, as streamlines within too close proximity could result in local over-extrusion. Volumetric coverage is used to compare the deposition path coverage relative to a more typical slicer that has no considerations for following an orientation field.

4.1. Topology Optimization Algorithm

TO is a family of optimization algorithms that develop an optimal distribution of material within a design space for a given set of loading and boundary conditions [36]. AM technologies have enabled more flexible use of TO through the additional geometric freedom provided by the fabrication processes [37]. The challenges of anisotropic mechanical properties are still present with these techniques though, leading to a number of TO formulations that take into account these properties [38]. Methods of propagating density features along paths of principal stresses (e.g., [39, 12]) inherently assign material orientations along those paths. Others, as previously discussed in Section 1.1, directly control the material orientation using design variables [7] or use concentric level-sets to define material orientation [9]. The authors' TO method, an extension of the method used in [7], simultaneously optimizes material distribution and orientation using design variables with direct control [16]. Although the algorithm allows for 3D material orientations, the optimization process was constrained to optimize orientations within the XY-plane to simplify the toolpath planning problem for this introductory work.

Table 1: Selected process parameters for validation of the VDPG algorithm.

Variable	Value	Description
d_{sep}	0.7	Seed point separation distance
d_{term}	0.4	Streamline termination distance threshold
d_{step}	1	Default integration step size
d_{lin}	0.2	Maximum allowable chord height
L_{min}	1	Minimum allowable streamline length
e	4	Element edge length

4.2. MBB Beam

The optimized beam (shown in Figure 8a) has a mesh size of 60 by 8 by 1 elements where each element has an edge length $e = 4$ units, producing a coarse structure with rapidly changing element orientations as they attempt to align with the load paths. In regions where different density features converge, the orientations are nearly orthogonal to each other. Even for this relatively simple structure, the orientation field is quite complex and does not necessarily follow the density features, which violates the assumptions made in existing orientation-informed path planners [7, 9]. Prescribing suitable shapes for the deposition paths throughout the design space (as required by [14]) would also be difficult.

The VDPG algorithm and mesh parameters used in this example are shown in Table 1, and the streamlines produced are shown in Figure 8c. To validate proper streamline termination, the distances between adjacent streamlines were calculated for each line segment (i.e., between each pair of integration points). The minimum distance between the spline-based streamlines was 0.2141 units, which is less than the chosen d_{term} but demonstrates that no streamlines overlap. Some of the streamlines do appear to overlap, but this is an artifact of the XY-projection of the 2.5D structure. These streamlines actually exist at different Z-heights within the structure. After linearization (shown in Figure 8d), the minimum distance decreased to 0.2091 units, showing that the linearization process also did not produce overlapping streamlines. The minimum distance could be driven closer to d_{term} (to maintain streamline spacing) by selecting a smaller integration step size or validating each intermediate integration point in the RK integrator.

The converging and diverging streamlines in the VDPG toolpath create voids that could weaken the resulting structure. To quantify the volume of these voids, the volumetric coverage of the geometry in deposition paths is calculated by sweeping a circle with a diameter equal to the anticipated deposition width and height (d_{sep}) along each linear path. The union of all of these swept paths constitutes the planned volume and accounts for overlapping deposition paths that are within d_{sep} of each other (i.e., overlapping regions are only counted once in the

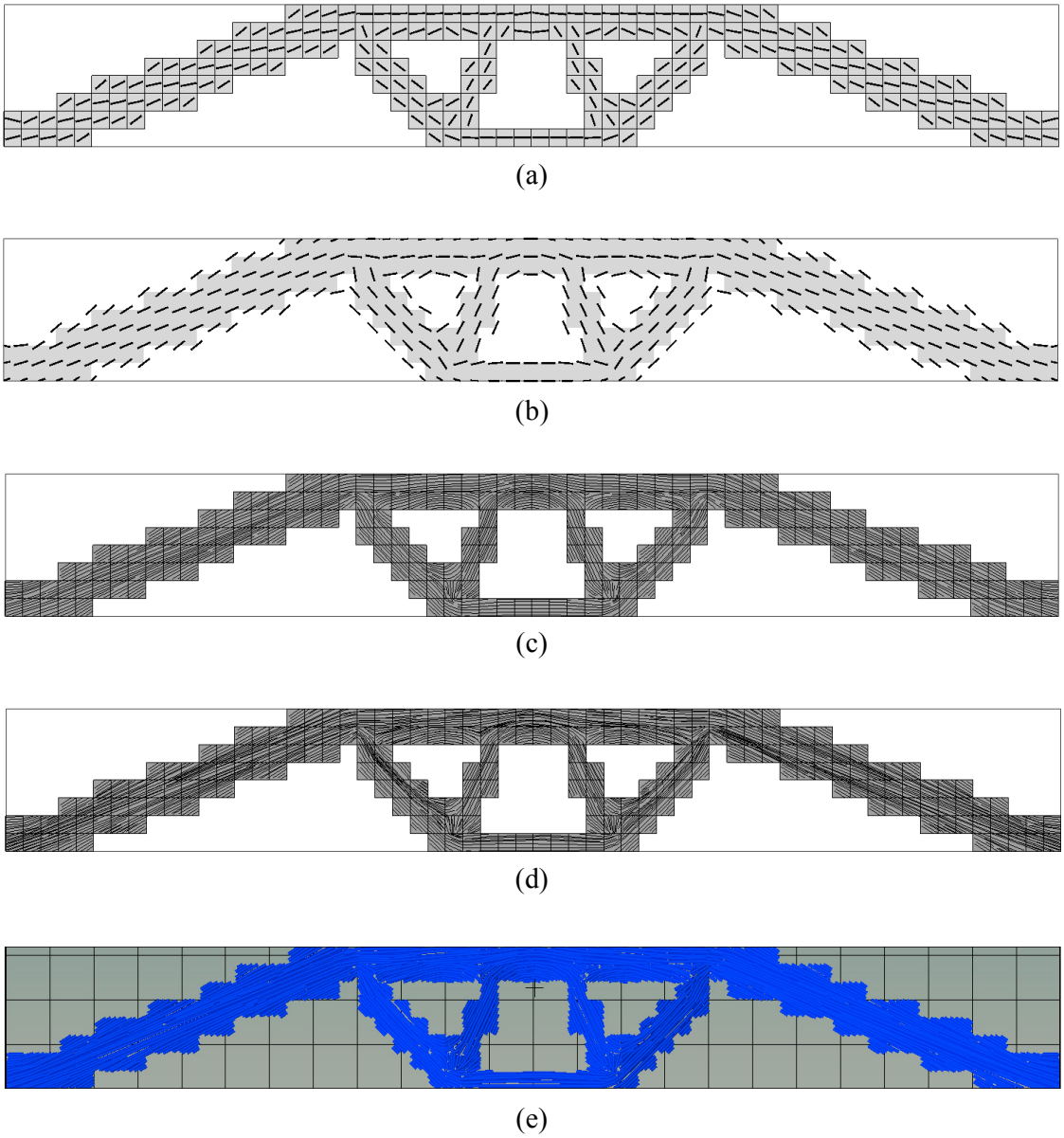

Fig. 8: VDPG algorithm applied to an optimized 2.5D MBB beam geometry. (a) the input structure and orientation field, (b) map the orientations to the nodes, (c) propagate streamlines through the structure, (d) linearize the streamlines for deposition, and (e) visualization of the final toolpath.

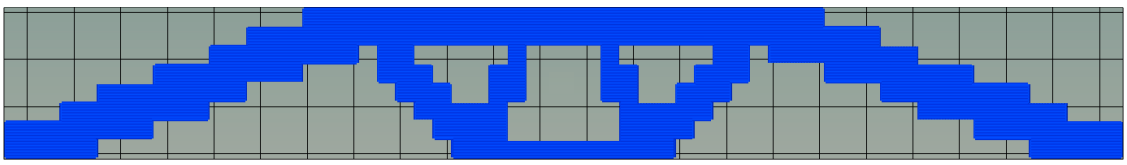

Fig. 9: Toolpath generated via Slic3r for the comparison of volumetric coverage.

planned volume). The volume covered by the planned deposition paths is 10300 cubic units, whereas the actual volume of the beam structure is 13312 cubic units, resulting in a volumetric coverage of 77.37%. The total volume of all the streamlines is 14979 cubic units, which means 31.24% of the total planned volume is overlapping and the structure will be over-deposited by 12.52%. For comparison, a toolpath for the same geometry was created with Slic3r [40] (shown in Figure 9) using the same process parameters but without accommodations for following the orientation field. Although the Slic3r toolpath appears to have complete volumetric coverage, the planned volume is 10210 cubic units with a volumetric coverage of 76.70%. There is no overlap in the planned volume, but there are gaps between the layers due to the low packing density of the layer-constrained deposition paths. As a result, the structure is under-deposited by 23.30% using Slic3r.

This issue of choosing between over- or under-deposition is common in ME toolpath planning; often small overlaps (i.e., a negative air gap) between deposition paths are advised for improving mechanical strength [3, 41]. This is due to the imperfect packing density of the deposition paths, which in the ideal case can achieve only a 90.7% packing density [42]. Ezair et al. demonstrated varying the deposition width, which should improve the packing density, but still produces small voids between adjacent depositions [14]. This is to say, changing the d_{term} parameter produces a similar behavior to changing the air gap in a typical slicer; volumetric coverage increases along with overlapping extrusions and the potential for over-deposition. Only one set of parameters was demonstrated in this work, but further optimization of the d_{sep} and d_{term} parameters is expected to improve the performance of VDPG.

Finally, a GCode toolpath, shown in Figure 8e, can be generated from the linearized deposition paths. Although the seeding array (Figure 6) does not produce layers like a typical slicer, each deposition path is still planar as a result of the planar orientation field. As such, a printable toolpath can be created by ordering the deposition paths in terms of ascending Z-height. Each point along the linearized streamlines was converted to a linear movement command with extrusion lengths and feed rates assigned using typical slicer parameters (e.g., road width, filament diameter, nozzle diameter, etc.).

5. Summary

The ME process produces parts with anisotropic mechanical properties due to the thermal characteristics of thermoplastic material deposition. By aligning deposition paths with stress-based orientation fields, part performance can be optimized, but the desired orientations can be quite complex depending on part geometry and performance requirements. Existing toolpath planning algorithms capable of generating deposition paths that follow these orientations are limited. Level set [9] and contour-based [7] methods are only applicable to orientation fields that follow the density features of the geometry, and existing volumetric approaches [14] rely on the deposition path shapes to be provided as input.

To alleviate these limitations, the authors present the volumetric deposition path generation (VDPG) algorithm, for volumetrically generating ME deposition paths, which is agnostic to both the geometry and orientation field without requiring predetermined path shapes. The VDPG algorithm leverages streamline placement algorithms commonly used for CFD flow field visualization to place volume-filling deposition paths throughout a structure that follow the desired orientation field. These spline-based streamlines are then linearized into deposition paths and ordered in terms of ascending Z-height to produce a printable toolpath.

A 2.5D MBB beam geometry (Figure 8), optimized in terms of both topology and material orientation [16], was used to validate the VDPG algorithm. Using the parameters outlined in Table 1, the algorithm produced a toolpath with deposition paths that covered 77.37% of the geometry's volume. For comparison, the same process parameters were given to a more traditional slicer, with no accommodations for following an orientation field, that produced a toolpath that covered 76.70% of the volume. Although the VDPG algorithm covers more of the volume, it plans to over-deposit the structure by 12.52%, implying a need to further tune the process parameters for a given road width. Regardless, the algorithm produced a printable toolpath that followed the desired orientation field with similar volumetric coverage to existing slicing tools.

Future work for the authors is focused on extending the VDPG algorithm to multi-axis geometries and fabricating the generated toolpaths. Multi-axis deposition enables the ability to tailor mechanical properties in full 3D, rather than being restricted to the XY-plane as with 3-DoF deposition. The optimal orientation fields for multi-axis printing become more complex, making a volumetric approach to toolpath planning, such as the VDPG algorithm presented here, promising for these platforms. The core of the VDPG algorithm is expected to remain unchanged when extending it to multi-axis deposition; streamline placement algorithms have already been demonstrated for 3D flow fields (e.g., [23, 24]). The main additional contributions required are i) a method for assigning a build direction to each deposition path and ii) a robust method for ordering the deposition paths. This ordering problem is more complex than in 3-DoF printing, as the deposition paths must be ordered such that previously deposited material does not prevent tool head access to unprinted regions of the structure. These issues are expected to be coupled as there are an infinite number of possible tool head orientations (i.e., build directions) that are perpendicular to each deposition path; some subset of these build directions should result in a possible collision-free ordering. From there, the authors look to quantify the mechanical performance benefits of multi-axis deposition with respect to 3D structures and parts.

6. Acknowledgments

The authors would like to thank the Institute for Creativity, Arts, and Technology at Virginia Tech for their financial support of this work.

References

[1] N. Guo and M. C. Leu, "Additive manufacturing: technology, applications and research needs," *Frontiers of Mechanical Engineering*, vol. 8, no. 3, pp. 215–243, 2013.

[2] J. E. Seppala and K. D. Migler, "Infrared thermography of welding zones produced by polymer extrusion additive manufacturing," *Additive Manufacturing*, 2016.

[3] S.-H. Ahn, M. Montero, D. Odell, S. Roundy, and P. K. Wright, "Anisotropic material properties of fused deposition modeling ABS," *Rapid Prototyping Journal*, vol. 8, no. 4, pp. 248–257, 2002.

[4] Z. Zhang and S. Joshi, "An improved slicing algorithm with efficient contour construction using STL files," *International Journal of Advanced Manufacturing Technology*, pp. 1347–1362, 2015.

[5] A. C. Brown and D. de Beer, "Development of a stereolithography (STL) slicing and G-Code generation algorithm for an entry level 3-D printer.," in *AFRICON*, 2013.

[6] H. Prüß and T. Vietor, "Design for Fiber-Reinforced Additive Manufacturing," *Journal of Mechanical Design*, vol. 137, no. 11, p. 111409, 2015.

[7] R. Hoglund and D. E. Smith, "Continuous Fiber Angle Topology Optimization for Polymer Fused Filament Fabrication," in *27th Annual International Solid Freeform Fabrication Symposium*, vol. 1, pp. 1078–1090, 2016.

[8] A. Michell, "The limits of economy of material in frame- structures," *Philosophical Magazine Series 6*, vol. 8, no. 47, pp. 589–597, 1904.

[9] J. Liu and H. Yu, "Concurrent deposition path planning and structural topology optimization for additive manufacturing," *Rapid Prototyping Journal*, vol. 23, no. 5, pp. 930–942, 2017.

[10] N. Boddeti, Z. Ding, S. Kaijima, K. Maute, and M. L. Dunn, "Simultaneous Digital Design and Additive Manufacture of Structures and Materials," no. September, pp. 1–10, 2018.

[11] W. S. Yerazunis, J. C. I. Barnwell, and D. N. Nikovski, "Strengthening ABS, Nylon, and Polyester 3D Printed Parts by Stress Tensor Aligned Deposition Paths and Five-Axis Printing," *Solid Freeform Fabrication Symposium*, pp. 1259–1271, 2016.

[12] K.-M. M. Tam and C. T. Mueller, "Additive Manufacturing Along Principal Stress Lines," *3D Printing and Additive Manufacturing*, vol. 4, no. 2, pp. 63–81, 2017.

[13] J. R. Kubalak, A. L. Wicks, and C. B. Williams, "Using multi-axis material extrusion to improve mechanical properties through surface reinforcement," *Virtual and Physical Prototyping*, pp. 1–7, 2017.

[14] B. Ezair, S. Fuhrmann, and G. Elber, "Volumetric covering print-paths for additive manufacturing of 3D models," *CAD Computer Aided Design*, vol. 100, pp. 1–13, 2018.

[15] C. Wu, C. Dai, G. Fang, Y. J. Liu, and C. C. Wang, "RoboFDM: A robotic system for support-free fabrication using FDM," *Proceedings - IEEE International Conference on Robotics and Automation*, pp. 1175–1180, 2017.

[16] J. R. Kubalak, A. L. Wicks, and C. B. Williams, "Topology Optimization to Enable Multi-Axis Material Extrusion Additive Manufacturing," *unpublished*.

[17] J. Donea and A. Huerta, *Finite Element Methods for Flow Problems.* John Wiley and Sons, Inc, 2003.

[18] G. Turk and D. Banks, "Image-guided streamline placement," *Proceedings of the 23rd annual conference on Computer graphics and interactive techniques - SIGGRAPH '96*, pp. 453–460, 1996.

[19] T. McLoughlin, R. S. Laramee, R. Peikert, F. H. Post, and M. Chen, "Over two decades of integration-based, geometric flow visualization," *Computer Graphics Forum*, vol. 29, no. 6, pp. 1807–1829, 2010.

[20] Z. Liu, R. J. Moorhead, and J. Groner, "An advanced evenly-spaced streamline placement algorithm," *IEEE Transactions on Visualization and Computer Graphics*, vol. 12, no. 5, pp. 965–972, 2006.

[21] O. Rosanwo, C. Petz, S. Prohaska, H. C. Hege, and I. Hotz, "Dual streamline seeding," *IEEE Pacific Visualization Symposium, PacificVis 2009 - Proceedings*, pp. 9–16, 2009.

[22] B. Jobard and W. Lefer, "Unsteady Flow Visualization by Animating Evenly-Spaced Streamlines," *Computer Graphics Forum*, vol. 19, no. 3, pp. 31–39, 2000.

[23] O. Mattausch, T. Theußl, H. Hauser, and E. Gröller, "Strategies for interactive exploration of 3D flow using evenly-spaced illuminated streamlines," *Sccg*, pp. 213–222, 2003.

[24] C. Rössl and H. Theisel, "Streamline embedding for 3D vector field exploration," *IEEE Transactions on Visualization and Computer Graphics*, vol. 18, no. 3, pp. 407–420, 2012.

[25] P. Alliez, D. Cohen-Steiner, O. Devillers, B. Levy, and D. Mathieu, "Anisotropic Polygonal Remeshing," *ACM Transations on Graphics*, vol. 22, no. 3, pp. 485–493, 2006.

[26] J. Zander, T. Isenberg, S. Schlechtweg, and T. Strothotte, "Creating High Quality Hatching Illustrations," *Computer Graphics Forum*, vol. 23, no. 12/2004, p. 2004, 2004.

[27] T. Wischgoll and G. Scheuermann, "Detection and visualization of closed streamlines in planar flows," *IEEE Transactions on Visualization and Computer Graphics*, vol. 7, no. 2, pp. 165–172, 2001.

[28] A. Mebarki, P. Alliez, and O. Devillers, "Farthest point seeding for efficient placement of streamlines," *Proceedings of the IEEE Visualization Conference*, p. 61, 2005.

[29] B. Jobard and W. Lefer, "Creating Evenly-Spaced Streamlines of Arbitrary Density," in *Visualization in Scientific Computing*, pp. 43–55, 1997.

[30] L. Li and H, "Image-based streamline generation and rendering," in *IEEE Transactions on Visualization and Computer Graphics*, vol. 13, pp. 1–11, 2015.

[31] B. Spencer, R. S. Laramee, G. Chen, and E. Zhang, "Evenly spaced streamlines for surfaces: An image-based approach," *Computer Graphics Forum*, vol. 28, no. 6, pp. 1618–1631, 2009.

[32] R. D. Cook, D. S. Malkus, M. E. Plesha, and R. J. W. Witt, *Concept and Applications of Finite Element Analysis*. USA: John Wiley & Sons, Inc., 2002.

[33] J. Horst and I. Beichl, "Efficient piecewise linear approximation of space curves using chord and arc length," in *SME Applied Machine Vision, Cincinnati, Ohio*, 1996.

[34] R. Rezaie, M. Badrossamay, a. Ghaie, and H. Moosavi, "Topology optimization for fused deposition modeling process," *Procedia CIRP*, vol. 6, pp. 521–526, 2013.

[35] A. T. Gaynor and J. K. Guest, "Topology optimization considering overhang constraints: Eliminating sacrificial support material in additive manufacturing through design," *Structural and Multidisciplinary Optimization*, vol. 54, no. 5, pp. 1157–1172, 2016.

[36] M. P. Bendsøe and O. Sigmund, *Topology optimization: theory, methods, and applications*. Springer, New York, 2003.

[37] T. Zegard and G. H. Paulino, "Bridging topology optimization and additive manufacturing," *Structural and Multidisciplinary Optimization*, pp. 175–192, 2015.

[38] P. Zhang, J. Liu, and A. C. To, "Role of anisotropic properties on topology optimization of additive manufactured load bearing structures," *Scripta Materialia*, vol. 135, pp. 148–152, 2017.

[39] T.-H. Kwok, Y. Li, and Y. Chen, "A structural topology design method based on principal stress line," *Computer-Aided Design*, vol. 80, pp. 19–31, 2016.

[40] "Slic3r." http://www.slic3r.org, November 2018.

[41] G. C. Onwubolu and F. Rayegani, "Characterization and Optimization of Mechanical Properties of ABS Parts Manufactured by the Fused Deposition Modelling Process," *International Journal of Manufacturing Engineering*, vol. 2014, pp. 1–13, 2014.

[42] A. Bezdek and W. Kuperberg, "Maximum density space packing with congruent circular cylinders of infinite length," *Mathematika*, vol. 37, no. 1, p. 7480, 1990.